

Insights into the strain history of Neoproterozoic limestones in the Paraguay Belt using stylolites

Kauê Seoane^{1*} , Fábio Henrique Garcia Domingos² 

Abstract

Tectonic stylolites are indicators of compressive deformation episodes in rocks and are commonly studied in terms of their geometrical attributes' length (L), and maximum (D_{max}) and average (D_{avg}) amplitudes. These parameters were analyzed for vertical stylolites from a sinistral strike-slip fault zone in limestones from the Guia Formation, Paraguay Belt, and compared mathematically to scarce vertical stylolites away from the fault zone. The study aimed to understand the role of strain-induced stylolites on the thinning of faulted limestone layers. Stylolites range from 2.66 up to 28.15 mm in length and from 0.143 up to 1.378 mm in amplitude. The total contractional strain (ϵ) was calculated for 49 stylolites with maximum amplitude peaks of 0.762 mm, using the Kostrov formula. The strain produced layer thinning and growth of the stylolite population. Regions of high stylolite concentration accommodated 16.92% contractional strain, whereas strain values of 3.29% are present in portions with low stylolite density. Layer thinning is directly proportional to contractional strain (ϵ) values spatially induced by faulting. The stylolite morphology plays an essential role in the permeability structure at the reservoir scale, where it can act as a barrier or a channel for fluid flux.

KEYWORDS: stylolites; Neoproterozoic; strain; Paraguay Belt; limestone.

INTRODUCTION

Deformation structures in rocks are an essential source of information to understand the tectonic history of a region. The study of microstructures helps to comprehend the deformation processes that affect rocks in two ways: to understand the mechanism(s) of deformation and to reconstruct the deformational framework (Passchier and Trouw 2004). Stylolites are structures present in fine-grained rocks, particularly in calcareous rocks (Dunnington 1954, Park and Schot 1968, Railsback 1993, André 2010, Rolland *et al.* 2012, 2014, Koehn *et al.* 2016). Stylolites exhibit teeth-like structures along their length, whose peaks relate to the magnitude of the stress they have undergone (Koehn *et al.* 2012, Ebner *et al.* 2009). In a recent study, Benedicto and Schultz (2010) obtained contractional strain values (ϵ) analyzing stylolite geometry and set a standard in the relation between fault zones and stylolites, as a function of strain accommodated by the layer.

The Northern Paraguay Belt in the south of the Amazonian Craton comprehends calcareous and siliciclastic successions from the Araras and Alto Paraguay groups, respectively, overlying a basement formed by metasediments from the Cuiabá Group (Nogueira *et al.* 2003). The history of deformation is

interpreted as the result of progressive deformation during a transpressional-transensional episode from the Neoproterozoic up to the Cambrian (Santos *et al.* 2020).

The stylolites in the Guia Formation limestones were studied at the microscopic scale to calculate indicative patterns of the total contractional strain (ϵ) caused by tectonic stresses. Strain calculation from stylolites in rocks is widespread (Ebner and Grasemann 2006, Koehn *et al.* 2007, Ebner *et al.* 2009, Benedicto and Schultz 2010, Rolland *et al.* 2012, Beaudoin *et al.* 2016, Koehn *et al.* 2016). This study investigated the relationship between sub-vertical stylolites and strike-slip faults in limestones by calculating strain values based on stylolite morphology. The role of stylolites as barriers or conduits for fluid flow was addressed.

Qualitative and quantitative methods were used to calculate the strain accumulated during the structural evolution of the Paraguay Belt and its implication for a hydrocarbon reservoir system.

THEORY

Stylolites: a review

Stylolites were first described by Klöden (1828) as structures related to organic species. At the beginning of the 20th century, Stockdale (1922, 1926) proposed these structures were individual columns (the teeth amplitudes), collecting insoluble materials along their suture, frequently associated with carbonates. He also suggested that the amplitude of a stylolite could represent the minimum thickness dissolution. Shaub (1939, 1949), Stockdale (1943), and Dunnington

¹Universidade de São Paulo – São Paulo (SP), Brazil. E-mail: kaue.seoane@usp.br

²Universidade Federal do Pará – Belém (PA), Brazil. E-mail: fabiohgd@ufpa.br

*Corresponding author.



(1954) proposed that pressure solution processes form stylolites after diagenesis. They considered the role of pressure in the solubility of the solids and differential solubility, as the critical factor to develop pervasive stylolites in carbonates (Shaub 1939, Passchier and Trouw 2004). Chemical heterogeneities, mineral solubility, and strain increase in rocks are the causes for stylolite formation (Renard and Dysthe 2003, Koehn *et al.* 2007, Brouste *et al.* 2007, Benedicto and Schultz 2010).

Stylolites are formed in a similar way to shear-enhanced compaction bands, where the propagation of large wavelengths results from strain increase (Tapp and Cook 1988, Katsman and Aharonov 2006, Schultz 2009, Schultz *et al.* 2013). Stylolite geometry is considered a fossil record of the deformation by registering the minimum values of strain magnitudes. Rock heterogeneities, including minerals with distinct composition, presence of mica lamellae, and other physico-chemical disturbances, control stylolite nucleation (Benedicto and Schultz 2010). Three types of stylolites are defined based on their genesis: sedimentary, bedding sub-parallel; tectonic stylolites, often perpendicular to the main compressive stress axis, typically intersecting bedding and previous sedimentary stylolites; and slickolites, which are tectonic stylolites that develop oblique to the main stress axis (Toussaint *et al.* 2018). The fractal roughness and dissolution rates during stylolite development are closely related and tend to cease when material dissolved from the sutures precipitates as a cement around the stylolite area (Ben-Itzhak *et al.* 2012).

Several studies relate volume changes during deformation to the formation of microstructures (Wright and Platt 1982, Ring *et al.* 2001, Sturm 2003, Ebner and Grasemann 2006). Deformed rocks often contain microstructures that can help understanding volume changes and mass transfer processes, that result from deformation. These microstructures include stylolites, pressure dissolution sutures, crenulation cleavage, and dissolution features around susceptible clasts (Ebner and Grasemann 2006).

GEOLOGICAL SETTING

The Paraguay Belt (Fig. 1A) comprises a sequence of metasedimentary rocks located along the southern border of the Amazonian Craton and east of the Rio Apa Block. The belt formed at 550–500 Ma, was intruded by the post-orogenic São Vicente Granite, and describes a convex arch toward the Amazon Craton with an approximate extension of 1,200 km (Almeida 1984).

Tectonic evolution

The Paraguay Belt formed during the Brazilian Cycle, constituted by metamorphic rocks overlaid by folded unmetamorphosed sedimentary rocks, is crosscut by brittle faults, and its evolution is generally described as polyphasal (Alvarenga 1988, 1990). The belt forms a regional scale convex arch toward the Amazonian Craton, showing reverse and thrusts faults, isoclinal and recumbent folds, with limited volcanic rocks and granitic intrusions in its inner part (Almeida 1984, Alvarenga 1990, Alvarenga & Trompette 1993). The Paraguay

Belt includes three structural domains: the Internal Zone encompassing pre-Ediacaran metasedimentary Cuiabá Group (Babinski *et al.* 2018), the External Zone containing the Puga Formation diamictites and the Araras and Alto Paraguay groups, and a Sedimentary Platform cover displaying gently deformed sedimentary rocks (Almeida 1964, 1984, Alvarenga & Trompette 1993).

Santos *et al.* (2020) proposes an evolution for the Paraguay Belt based on progressive deformation where two successive transpressional-transtensional episodes took place. The early ductile to brittle-ductile transpressional deformation affected only the metasedimentary rocks of the Cuiabá Group in the southeastern part of the belt, producing a regional E-W to NE-SW trending foliation. The later brittle transtensional deformation episode formed oblique-normal and strike-slip faults and joints following the trends NE-SW, NW-SE, N-S, and E-W. The relatively younger rocks from Puga Formation, Araras and Alto Paraguay Groups, display no evidence of ductile structures (Santos *et al.* 2020).

Sedimentary cover

The Paraguay Belt comprises a basement of metamorphic rocks of the Cuiabá Group, including phyllites, quartzites, metagraywackes, and metaconglomerates (Alvarenga & Trompette 1994), overlaid by the sedimentary rocks of the Paraguay Basin formed by Marinonan glacial diamictites, siltstones, and sandstones of the older Puga Formation covered by the Araras Group carbonates. These rocks are covered by the siliciclastics of the Alto Paraguay Group in the basin (Alvarenga *et al.* 2004, Nogueira 2003).

The Araras Group includes four formations:

- The oldest Mirassol d'Oeste Formation comprising fine dolostones, and shallow platform peloidal dolostones;
- Guia Formation formed by bituminous limestones, shales, pellets, and cementstones with flat lamination interrupted by breccia and slope related deformation, indicating a low energy platform sedimentation;
- Serra do Quilombo Formation, composed of fine dolomites, breccias with dolomitic cement, and sandy dolomites with hummocky cross-stratification, deposited in a platform;
- Nobres Formation including dolomites, sandstones, pelites with levels of silex and oolitic and sandy dolomites formed in tidal/sabkha plains environment (Nogueira 2003).

The siliciclastic rocks of the Alto Paraguay Group lying above the Araras Group comprise the formations: Raizama, formed by sandstones and mudstones; and Sepotuba, composed of mudstone, shales, sandstones, red rhythmites, and conglomerates (Silva Júnior *et al.* 2007). U-Pb ages in zircons of the youngest Diamantino Formation suggest a maximum sedimentation age of 541 ± 7 Ma, for the Alto Paraguay Group extending from the lower Cambrian (Silva Júnior 2011).

Lacerda Filho *et al.* (2001) proposed that the older chemical sedimentary rocks of the Paraguay Belt represent products of a redox sedimentary environment in a deep Passive Margin, and the younger siliciclastic belong to a sedimentary sequence deposited in a Foreland Basin.

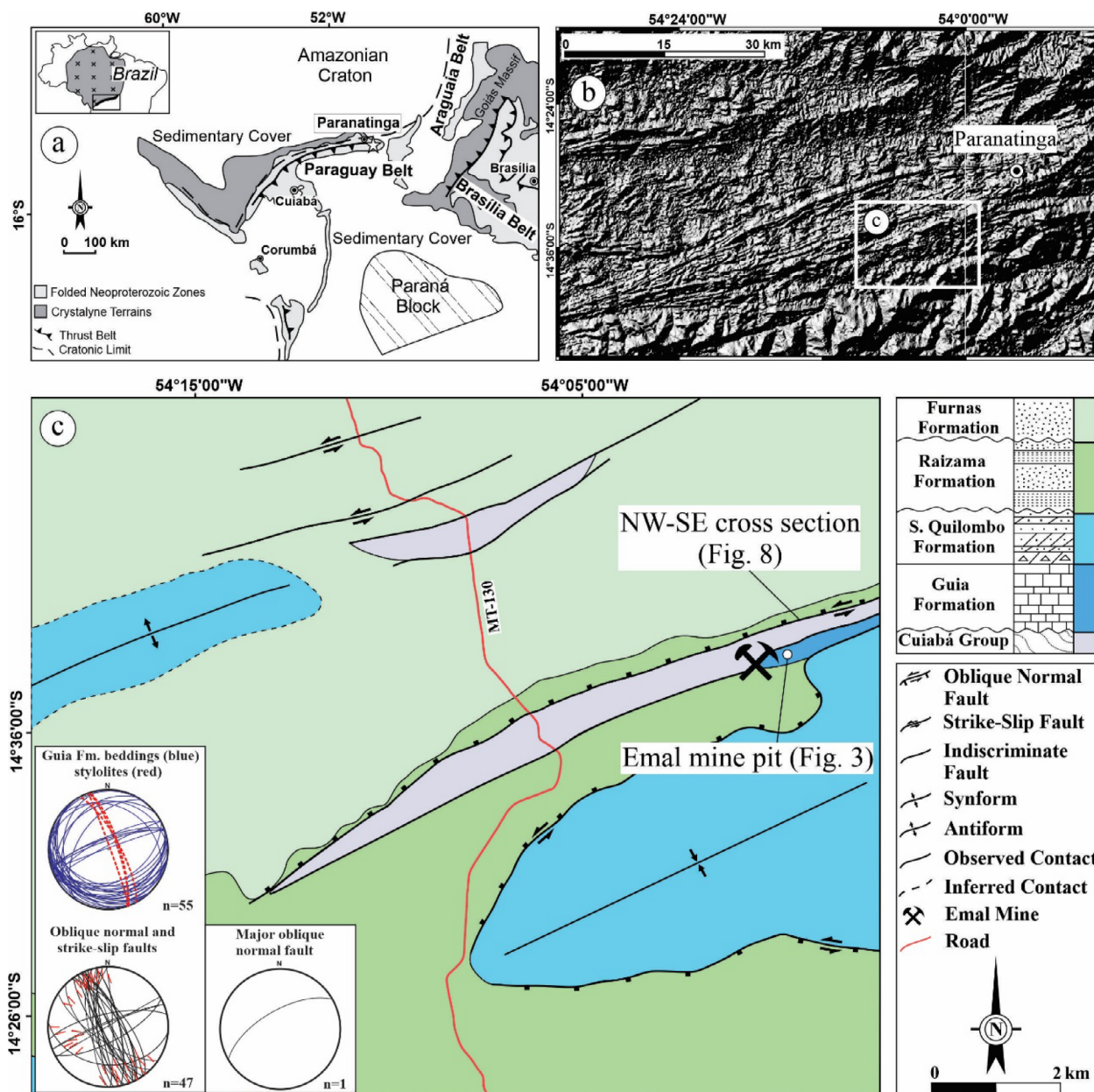


Figure 1. (A) Simplified tectonic map of the Tocantins Province, showing the Paraguay Belt, and other regional tectonic members, Araguaia and Brasília belts, and Goiás Massif. Star represents the location of the studied area near the town of Paranatinga (adapted from Pimentel *et al.* 2000). (B) Shaded relief (30 m resolution Digital Elevation Model, Farr *et al.* 2007) image from the east section of the Paraguay Belt, including Paranatinga town, showing prominent NE-SW lineaments, cross-cut by later NNW-SSE lineaments. White rectangle indicates the location of (C). (C) Geological map of the studied area exhibiting geological units and major structures (e.g. oblique normal and strike-slip faults). Stereograms show bedding (solid blue), stylolites (dashed red), and faults as great circles.

We studied dark grey, finely laminated limestones of the Guia Formation inside of the Emal-Paranatinga quarry (Figs. 1B and 1C). They are mudstones formed by carbonate mud, with quartz and subordinate muscovite.

METHODS

The study was carried out in the Emal-Paranatinga quarry, which lies in the Guia Formation calciferous limestones, crosscut by WNW-ESE and NW-SE trending faults. The block studied is situated in the inner part of a sinistral strike-slip fault zone displaying tectonic stylolites sub-orthogonal to the sedimentary layering (Fig. 1C, stereonet).

Two samples from the inner part of the fault zone (CP-01 and CP-02) and two from outside (CP-03 and CP-04) were studied using thin sections (Fig. 2). Amplitude and length measured in the stylolites aided the calculation of the total contractional strain (ϵ) in the area of the thin section. Samples CP-03 and CP-04, away from the fault zone (Fig. 3), show no or few stylolites or little evidence of dissolution at the grain scale, which allowed us to calculate the standard value of thinning to obtain the ratio between those strain values. The amount of thinning is given by Equation 1:

$$\epsilon_{\text{layer}} = \Delta T / T_0 \tag{1}$$

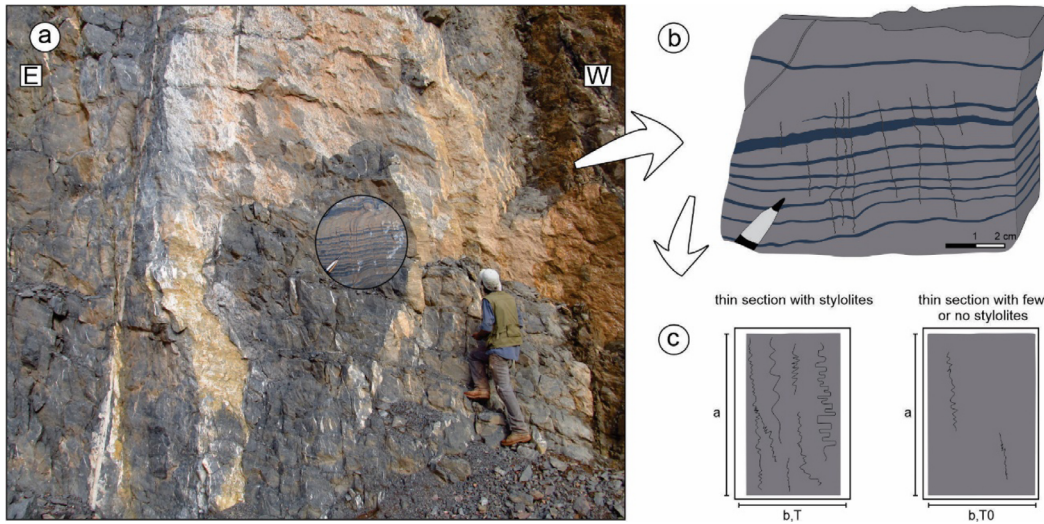


Figure 2. (A) Outcrop showing the sub-vertical fault zone and the studied limestone block of the Guia Formation in the Emal-Paranatinga quarry (14°33'45.56"S; 53°57'32.81"W). Bedding is dipping gently to the right. Inset circle represents the sample location, CP-01/02. (B) Schematic diagram of the mudstone study block displaying the spatial relation between horizontal layers and perpendicular stylolites. (C) Thin section representation showing the traces of the analyzed stylolites (CP-01 and CP-02) where the T (final stage) is obtained; and with few or no stylolites (CP-03 and CP-04) where T_0 (initial stage with no or few dissolution structures) is obtained and provide the ΔT . Dimensions a and b were used to calculate the total area of the thin sections for the thin section strain calculation (Tab. 3).

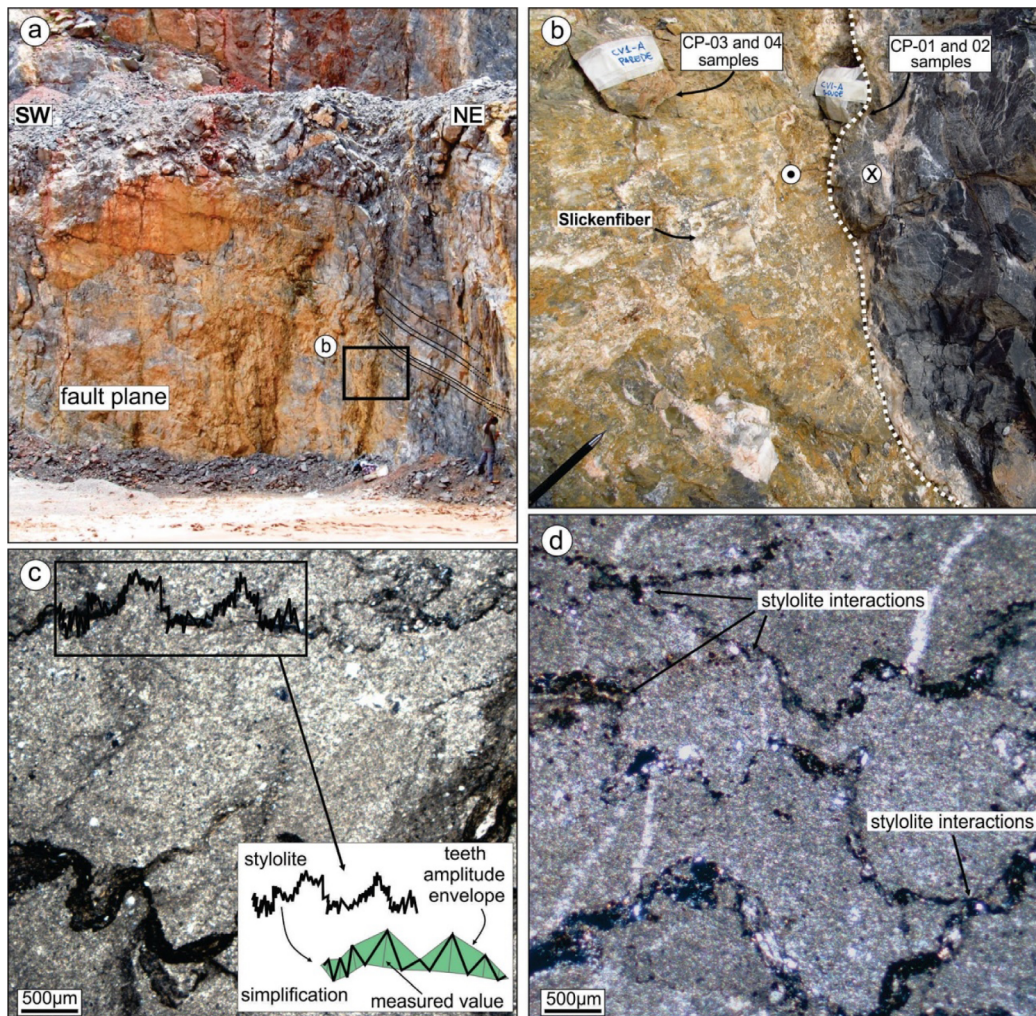


Figure 3. (A) Sub-vertical fault plane showing irregular geometry and gently dipping bedding. (B) Calcite slickenfibers on the fault plane indicating sinistral kinematics for the strike-slip fault. Location of the study samples from the fault zone (CP-01 and CP-02) and from the fault footwall (CP-03 and CP-04). Calcite veining is noticeable in the fault zone and onto the fault plane forming slickenfibers. (C) Microphotograph of mudstone and stylolites showing the graphical procedure for measuring the geometrical features of individual stylolites (0.5 mm). (D) Microphotograph detail displaying the interactions between stylolites, linking their sutures (0.5 mm). Stylolites in c and d are stylolites perpendicular to the sedimentary bedding (Fig. 2).

Where:

ΔT = the reduction in layer thickness measured from the inside to the outside of the fault zone.

T_0 = 40 mm without shortening (CP-03 and CP-04), showing no or few stylolites (Tab. 1).

The results of the layer thinning (ϵ_{layer}) calculation are shown in Tables 2 and 3.

Table 1. Thin sections dimensions and areas. In the thin sections with many stylolites, only the area encompassing stylolites was used in the calculation, while the entire area of the thin section was used in the others. The value of T_0 for calculation purposes was obtained from samples 03 and 04. All thin sections assume original thickness $T_0 = 40$ mm with measurement uncertainties of ~ 3 mm.

Samples	Description	T (mm)	A (mm ²)
01 and 02	Many stylolites	29.52	1,180.8
03 and 04	Few or no stylolites	40.0	1,600.0

Table 2. Stylolites dimensions and ratio relationship between their elements.

Stylolite	Total Length, L (mm)	D _{AVG} (mm)	D _{MAX} (mm)	D _{AVG} /L	D _{MAX} /L
S1	5.25	0.104	0.144	0.0198095	0.0274286
S2	6.37	0.151	0.242	0.0237049	0.0379906
S3	3.97	0.153	0.241	0.038539	0.0607053
S4	3.95	0.085	0.143	0.021519	0.0362025
S5	36.7	0.218	0.603	0.0059401	0.0164305
S6	3.05	0.329	0.576	0.1078689	0.1888525
S7	7.4	0.291	0.472	0.0393243	0.0637838
S8	6.34	0.266	0.361	0.0419558	0.0569401
S9	10.34	0.264	0.468	0.0255319	0.0452611
S10	8.37	0.243	0.762	0.0290323	0.0910394
S11	16.35	0.199	0.357	0.0121713	0.0218349
S12	7.67	0.135	0.211	0.017601	0.0275098
S13	17.95	0.281	0.565	0.0156546	0.0314763
S14	24.4	0.354	0.719	0.0145082	0.0294672
S15	7.44	0.344	0.637	0.0462366	0.0856183
S16	8.85	0.218	0.536	0.0246328	0.060565
S17	10.23	0.155	0.218	0.0151515	0.0213099
S18	16.57	0.266	0.601	0.0160531	0.0362704
S19	2.66	0.171	0.245	0.0642857	0.0921053
S20	12.09	0.318	0.584	0.0263027	0.0483044
S21	11.9	0.378	0.489	0.0317647	0.0410924
S22	10.52	0.442	0.829	0.0420152	0.0788023
S23	28.15	0.595	1.378	0.0211368	0.048952
S24	15.77	0.566	1.041	0.0358909	0.0660114
S25	17.63	0.456	1.101	0.025865	0.0624504
S26	5.09	0.401	1.012	0.0787819	0.1988212
S27	4.52	0.331	0.488	0.0732301	0.1079646
S28	3.7	0.527	0.663	0.1424324	0.1791892
S29	6.07	0.432	0.658	0.0711697	0.108402
S30	3.46	0.227	0.384	0.0656069	0.1109827
S31	4.57	0.256	0.382	0.0560175	0.0835886
S32	3.84	0.417	0.561	0.1085938	0.1460938
S33	4.1	0.963	1.011	0.234878	0.2465854
S34	7.17	0.179	0.41	0.0249651	0.0571827
S35	27.45	0.391	1.25	0.0142441	0.0455373
S36	18.86	0.427	0.71	0.0226405	0.0376458
S37	5.87	0.151	0.35	0.025724	0.0596252
S38	9.02	0.483	0.564	0.0535477	0.0625277
S39	11.95	0.414	0.75	0.0346444	0.0627615
S40	5.52	0.262	0.32	0.0474638	0.057971
S41	28.35	0.418	0.935	0.0147443	0.0329806
S42	7.56	0.232	0.42	0.0306878	0.0555556
S43	8.76	0.358	0.72	0.0408676	0.0821918
S44	12.81	0.755	1.358	0.0589383	0.1060109
S45	12.52	0.502	1.22	0.0400958	0.0974441
S46	12.44	0.757	1.62	0.0608521	0.1302251
S47	22.07	0.434	1.08	0.0196647	0.0489352
S48	8.03	0.263	0.564	0.0327522	0.0702366
S49	7.75	0.422	1.27	0.0544516	0.163871

Table 3. Contractional strain in the thin sections within and out of the damage zone.

Samples	Description	Layer thinning strain (%)	Stylolites strain (%)	Stylolite/Layer thinning (%)
01 and 02	Many stylolites	26.2	16.92	64.8
03 and 04	Few stylolites	0	3.29	-

Samples CP-01 and CP-02 show stylolites, quantitatively analyzed by measuring their dimensions (length and amplitude), in microphotographs. The measurements from a total of 49 stylolites consist of 33 stylolites from sample CP-01, and 16 from sample CP-02 (Fig. 4).

We applied the carbonate rock classification by Dunham (1962), and the stylolites amplitude measurements follow the procedures described by Benedicto and Schultz (2010), defined as the distance between the peak of the stylolites in the envelope to its base measured along a perpendicular line (Fig. 3C). The length was measured along the curved trace of the stylolites (Fig. 3C).

The total contractional strain (ϵ) perpendicular to the stylolites results from the sum of amplitude and length of all the stylolites divided by the entire area of the two studied thin sections, following the methods used in structural geology, seismotectonic, and comparative planetology (Molnar 1983, Scholz and Cowie 1990, Scholz 1997, Schultz 2003, Benedicto and Schultz 2010). Equation 1, by Kostrov (1974), allows calculating strain values from the “seismic moment” and the total contractional strain value (ϵ) (Eq. 2):

$$\epsilon = \frac{1}{A_0} \sum_{i=1}^N D_i L_i \quad (2)$$

D_i = the average amplitude;

L_i = stylolite length;

A_0 = the area of the thin section.

This formula provides valid strain values based on amplitude and length of stylolites. The D_i value comes from measurements following the example in Figure 2D, where the amplitude comprises the maximum value perpendicular to the envelope drawn around the stylolite. The total stylolite length gives the L_i value from tip to tip, and A_0 was calculated from the total area of the two thin sections.

RESULTS AND DISCUSSION

The mudstones of the Guia Formation, in the damage zone of the NE-SW sinistral strike-slip fault (Figs. 3A, and 3B), present stylolites analyzed morphologically based on their amplitude and length (Fig. 3C) and some interactions between them (Fig. 3D; the thin sections represent a horizontal section perpendicular to the stylolites). Mudstones are dark grey, characterized by gentle plane lamination (Fig. 2) and scattered fine-grained quartz grains in a microcrystalline matrix (Fig. 4). Breccias, veins (Fig. 4), micro faults, and stylolites are present in the samples from the damage zone (Fig. 3B). The stylolites are perpendicular to the sub-horizontal mudstone bedding (Fig. 2) indicating their tectonic origin. Carbonate layers trend NE-SW, dipping gently NW, but those crosscut

and dragged by oblique normal and strike-slip faults (NE-SW and NW-SE) show steep dips and follow the regional structural trend observed in the DEM for the area (Figs. 1B and 1C — stereograms).

The total contractional strain (ϵ) value was calculated by summing the contributions of each stylolite and dividing this sum by the original area of the layer (Benedicto and Schultz 2010). Layer thinning percentage is connected to the total contractional strain (ϵ). Overall, these findings agree with the results reported by Benedicto and Schultz (2010), showing a correlation between increasing contractional strain and layer thinning.

Stylolite morphology

The morphology of stylolites includes length (L) and amplitude (D), with variable values according to the geometry. We analyzed 49 stylolites (Figs. 3 and 4), where CP-01 and CP-02 samples from inside a fault zone have a higher density of stylolites than the CP-03 and CP-04 samples away from the fault zone. The stylolites outside of the fault zone exhibit lower amplitudes and overall length than those from inside of the fault zone.

Morphologically, the stylolites present shapes similar to teeth or blades (Fig. 3C) that control their symmetry and distinguish them from other microstructures (Renard *et al.* 2004). Stylolite length ranges from 2.66 to 36.7 mm in the studied block. They display asymmetric undulating surfaces, with amplitudes varying from 0.037 to 1.358 mm. The stylolite interior typically has mineral filling showing insoluble quartz grains, micas, mudstone fragments, calcite vein fragments, green clay minerals, and black amorphous material microscopically similar to iron oxide, which can reach thicknesses of up to 0.6 mm in some parts of the stylolites. The relative concentration of insoluble phases individually defines the local solubility rate and is associated with the contractional strain rates, generating the stylolitic morphologies observed in the samples (Benedicto and Schultz 2010).

The further growth of some stylolites produces an interconnected anastomosing pattern of long and continuous stylolites with implications for the permeability of the rock and fluid flow (see Fig. 4 S11, S10, S18, S24, S26, S29, S32, S34, S35, S37, S41, S42, and S47) (Ben-Itzhak *et al.* 2014). The surface morphology and nature of minerals filling the structures, control whether they function as seals or channels for fluid flow. The concentration of impermeable materials in the structure creates a barrier. The offsetting of existing structures facilitates fluid flow, tearing down existent barriers in the stylolite wall and causing their peaks to seal (Koehn *et al.* 2007, 2016). Data show a significant number of the Koehn's class seismogram pinning type stylolite (see Fig. 4 stylolites S5, S8, S14, S18, S23, S24, S29, S32, S34, S35, S36, S38, S44, S45, and

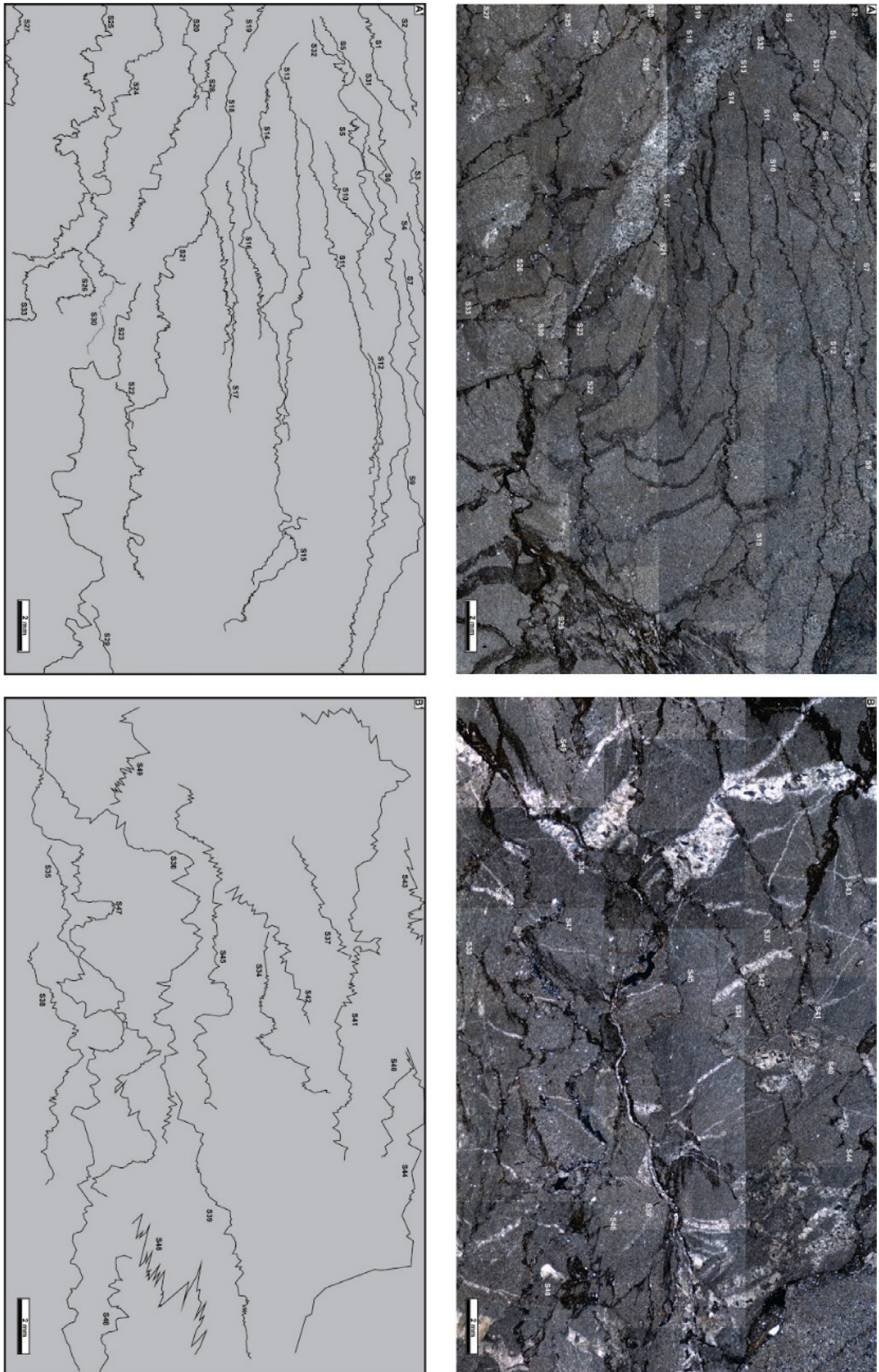


Figure 4. Panoramic microphotographs of the study thin sections and respective stylolite map where amplitude and length measurements were taken for individually numbered stylolites. (A) CP-01 sample showing 33 stylolites. (A') CP-01 stylolite map with numbered stylolites. (B) CP-02 showing 16 stylolites. (B') CP-02 stylolites map drawn and respective numbers.

S47) (Koehn *et al.* 2016). These stylolites might be a barrier, depending on how much sealing material is present on the median surface. Nevertheless, if these stylolites present rough teeth, it might suggest the sealing material, if collected, will be displaced along their surface and a circulating fluid could leak across teeth flanks due to these vertical teeth being parallel to the main stress direction (compression), thus creating a favorable pathway to the fluid circulation (Bruna *et al.* 2019).

Moreover, many studies have advocated an increase in porosity as a result of stylolite development, linking their morphology features, such as flank and the tip of the stylolite, to enhanced fluid flow (Carozzi and Vonbergen 1987, Dawson 1988, Raynaud and Carrio-Schaffhauser 1992, Van Geet *et al.* 2000, Gingras *et al.* 2002, Harris 2006, Toussaint *et al.* 2018).

Morphologically, the stylolites are grouped into three classes based on visual characterization of their amplitude and length values. Symmetric stylolites present fairly regular structures with no well-defined amplitude peaks (see blue stylolites in Fig. 5: S2, S3, S5, S6, S19, S20, S23, S24, S27, S35, S36, S38, S41, S42, and S47). Asymmetric stylolites exhibit variation in amplitude along their length and subordinate amplitude peaks (see yellow stylolites in Fig. 5 S7, S10, S12, S16, S18, S21, S22, S23, S25, S26, S29, S30, S33, S34, S37, S43, S46, and S48). Incongruous stylolites show no clear relation between amplitude and length (see orange, pink, and gray stylolites in Fig. 5 S1, S3, S4, S8, S9, S11, S13, S14, S15 S17, S28, S31, S32, S39, S40, S44, S45, and S49).

Total contractional strain (ϵ)

Total contractional strain (ϵ) was estimated from all thin sections, including those with few or no stylolites values. Strain was summed for the pairs of samples, with numerous (CP-01 and 02) and few (CP-03 and 04) stylolites, to compare the data and analyze contractional strain in each case.

The results from strain measurements in the layer (Tab. 1) are the basis for evaluating the total contractional strain (ϵ) accommodated during the development of stylolites. The data from the layer were part of the calculation presented in Table 3.

The total contractional strain (ϵ) was obtained based on values of amplitude and length of the stylolite sets in the layers. The scalar ratio between average amplitudes and total length allowed to estimate the role of deformation in developing stylolites on carbonates (Benedicto and Schultz 2010). These values represent the minimum contraction strain in the rocks as they result from calculations using only morphologically favorable stylolites (> 85% of those present in the samples). Thus, the value has at least 15% of uncertainty caused by the thinning accommodated by pressure dissolution during the deformation.

Regionally, the deformation history in the Paraguay Belt comprises a polyphase deformation hypothesis characterizing three structural domains (Almeida 1964, 1984, Alvarenga & Trompette 1993). An alternative model explains the deformation in the belt based on two successive transpressional and transtensional events under conditions compatible with ductile and brittle-ductile regimes, respectively (Santos *et al.* 2020). The studied limestones display faults and joints formed

during a brittle transtensional (partitioned) event that affected both basement and sedimentary rocks (Santos *et al.* 2020). Structural data recorded in the Emal-Paranatinga quarry show NE-SW and NE-SW trending oblique faults (as shown in stereonet in Fig. 1). These fault families agree with the regional structural framework described in Santos *et al.* (2020) for brittle structures formed during regional transtension. The inclined stylolites observed in NE-SW fault zones indicate they developed due to the strain accommodated during the evolution of these faults. They are distinct in origin from the bedding parallel stylolites, related to diagenetic processes and commonly observed in limestones.

Percentage of layer thinning

The thicknesses of the analyzed layers decrease progressively as the stylolites concentration increases in the thin section (Tab. 1). Layer thickness changes from $T_0 = 40$ to 29.52 mm toward the fault zone, indicating a contractional strain of 26.1% (Tab. 3), accommodated by the rocks in the damage zone. This finding agrees with a previous work by Benedicto and Shultz (2010) near the Gubbio Fault, Central Italy, where they argued that stylolites developed from fault-related layer thinning.

The Kostrov formula (see Methods) gave layer thinning results ranging from 3.29% in areas with few stylolites, to 16.92%, where several stylolites are present in the samples. Strain accommodation induces stylolite growth more efficiently toward the fault zone, where higher layer thinning is accordingly seen. The highest concentration of stylolites indicates that the contractional strain accommodated by layer thinning was ~60 times the value of the maximum amplitude of the stylolites measured. The ratio between the percentage of strain in stylolite and the thin section indicates that the stylolites accommodated 64.8% of the total strain estimated from the layer thinning.

Around 60% of the visible thinning is related to strain accommodated by stylolites, meaning that other mechanisms probably accommodated the rest of the volume loss, most likely the development of brittle structures such as veins (Fig. 4), breccias, and microfractures. However, the 60% volume change (3/5 ratio) disagrees with that presented by Benedicto and Schultz (2010), as their results indicate a 20% thinning related to stylolite development in the layer, and 80% due to brittle strain. The disparity is probably caused by the 40 analyzed stylolites in this study, against 18 in the former. Nevertheless, this is the only relevant difference between both studies using the same method, which seems satisfactory, in terms of contractional strain accommodation by stylolites in faulted layers. Our results reveal that significant layer thinning was accommodated by stylolites development, from portions with absent or little thinning up to 26.1% thinning (Fig. 6).

Displacement-length scaling relation

Stylolite morphology allowed us to analyze two relations between displacement-length ($D-L$) = D_{max}/L and D_{avg}/L , where D_{max} represents the maximum amplitudes of a stylolite, D_{avg} corresponds to the average amplitude, and L comprises

the total length for each stylolite. In both cases, D is related to the displacement for each stylolite plane. 40 out of 49 stylolites with reliable amplitude and length values are on the graphic in Figure 7.

The log-log plot of maximum amplitude *versus* length (D_{max}/L), provides the equation $D_{max} = 0.0066L^{0.5}$ and $r^2 = 0.3$ (Fig. 6). Though the limited range in the length for our samples should be considered, the slope of ~ 0.5 indicated for our

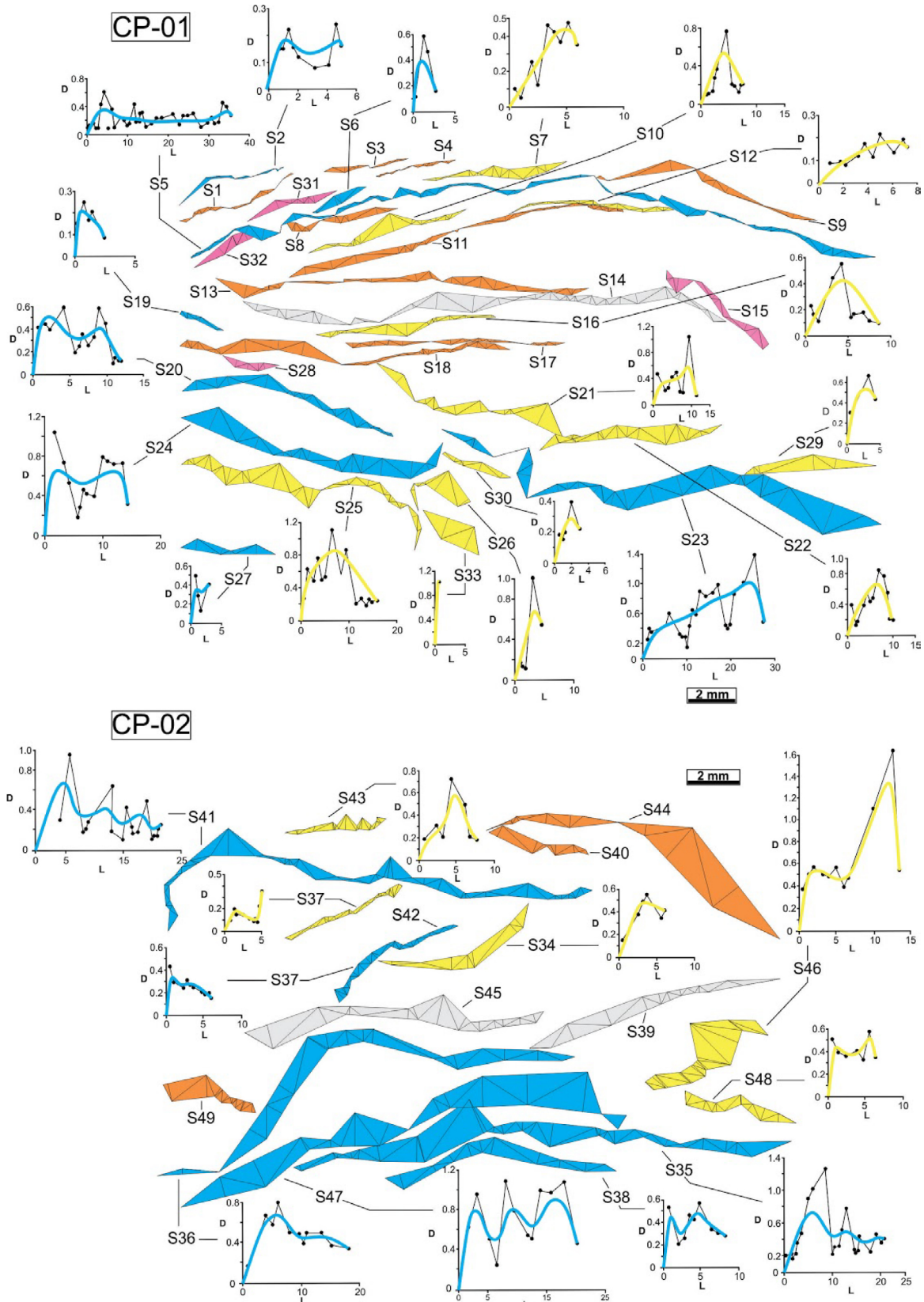


Figure 5. Map of the stylolites in mudstones from samples CP-01 and CP-02, with plots of amplitudes versus total length for each stylolite measured (scale in millimeters). Symmetric stylolite are blues, asymmetric are yellow, and incongruous are orange, pink and gray. The others graphics are shown in the Appendix 1.

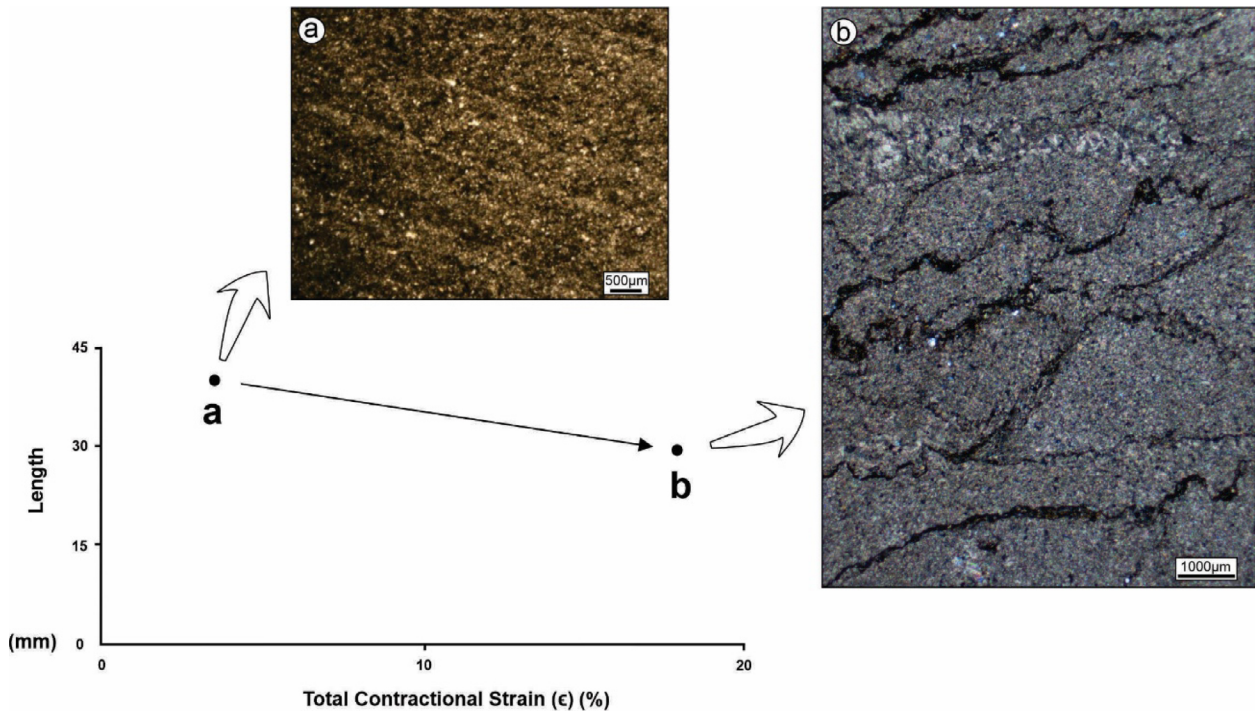


Figure 6. Length versus Total Contractural Strain (ϵ) plot for samples analyzed for a single layer. Point *a* represents an area of sample CP-03 with limited deformation, thus virtually no layer thinning, and point *b* represents sample CP-01 with a relatively high number of stylolites. The total contractural strain (ϵ) increases from *a* to *b*. Length in mm.

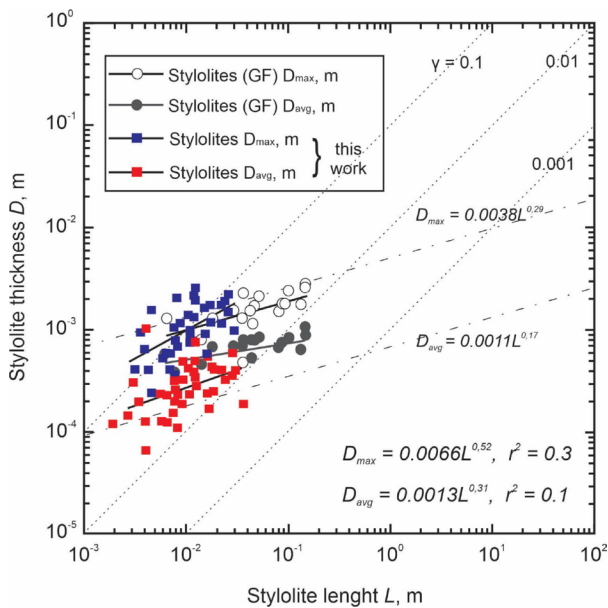


Figure 7. Stylolite displacement-length (thickness-length) scaling relations for 40 stylolites in mudstones from the Emal-Paranatinga quarry. For correlation, Benedicto and Schultz (2010) data from stylolites in Gubbio Fault (GF), Central Italy. Constant slope lines are $n = 1$, dotted, characteristic of faults: $D/L = \gamma$, $n = 0.5$, and dashed, characteristic of Gubbio stylolites.

D_{max} curve is higher than the ~ 0.3 value found by Benedicto and Schultz (2010) in limestones close to the Gubbio Fault, central Italy, but similar to the ~ 0.5 value reported for shear-enhanced compaction bands (Sternlof *et al.* 2005, Schultz 2009). A similar pattern of results was obtained for opening fractures

such as joints, veins, and igneous dikes (Olson 2003, Schultz *et al.* 2008, Klimczak *et al.* 2010); and cataclastic deformation bands (Fossen and Hesthammer 1997).

The stylolites show an irregular pattern in the distribution of maximum topography amplitudes, making it difficult to observe individual displacements. This limitation prevented the use of D_{max}/L results for calculating contractural strain values. This finding is directly in line with previous works of Benedicto and Schultz (2010) and Koehn *et al.* (2007), where we see similarities in results. They proposed that physico-chemical heterogeneities are as important as the contractural strain to develop stylolites.

The log-log plot for amplitude average *versus* length for individual stylolites (D_{avg}/L) as log-log (see black squares on Fig. 6) provides the equation $D_{avg} = 0.0013L^{0.3}$, although with a low r^2 of 0.1. The values have relevance in estimating volume loss and values of the contractural strain accommodated by stylolites. The study by Benedicto and Schultz (2010) has demonstrated that this scaling relationship does not consider the effects of rock heterogeneities and reflects the mechanical response resulting from local dissolution processes on the stylolite length.

Benedicto and Schultz (2010) demonstrated that the average amplitude values (which links to the stylolites topography) are related to the length values, resulting from an increase in contractural strain accommodated by stylolites, along with the scale exponent value 0.3. Contrary to Olson (2003) findings, values of 0.5 show fracture growing under constant driving stress conditions. The scale exponent value obtained for fault-related stylolites in the mudstones at Emal-Paranatinga

quarry pit indicates that the increase in stylolite topography was proportional and took place at different rates. The high-amplitude and long-length stylolites observed in this study were formed with the progressive development of their morphology, contrasting with Benedicto and Schultz's (2010) value of 0.17, indicative of long-length and low-amplitude stylolites.

The asymmetry of our stylolites shown by the relation between amplitude and length (Fig. 5) may indicate that they propagated from the more thinned to the less thinned layer, which according to Benedicto and Schultz (2010) and Brouste *et al.* (2007) suggests that contractional strain increased progressively during their growth and the peaks of maximum amplitude account to areas in the layer that present physico-chemical heterogeneities.

CONCLUSIONS

A quantitative analysis of stylolites, investigating the displacement-length relationship according to morphological

measurements, improved the comprehension of stylolites development and the amount of contractional strain in carbonates in the wallrock of a sinistral strike-slip fault. The maximum amplitude and length of these structures increased proportionally with the increase in contractional strain. Our findings agree with previous work on stylolite-related contractional strain (Benedicto and Schultz 2010), statistical analyses of stylolite morphology (Karcz and Scholz 2003, Peacock and Azzam 2006), and numerical simulations of stylolite growth (Koehn *et al.* 2007).

The NE-SW trending sinistral strike-slip fault studied in this work accommodated sufficient contractional strain (ϵ) to develop the set of tectonic stylolites observed, producing a permeability anisotropy with important implications for fluid flow and migration in a reservoir. The approximate NW-SE orientation of the extensional strain (Fig. 8), is compatible with the spatial position of the NE-SW oblique-normal faults. The NW-SE tectonic stylolites suggests a local NE-SW maximum compressive stress, which caused the dissolution of the limestones and development of the stylolites. From a regional

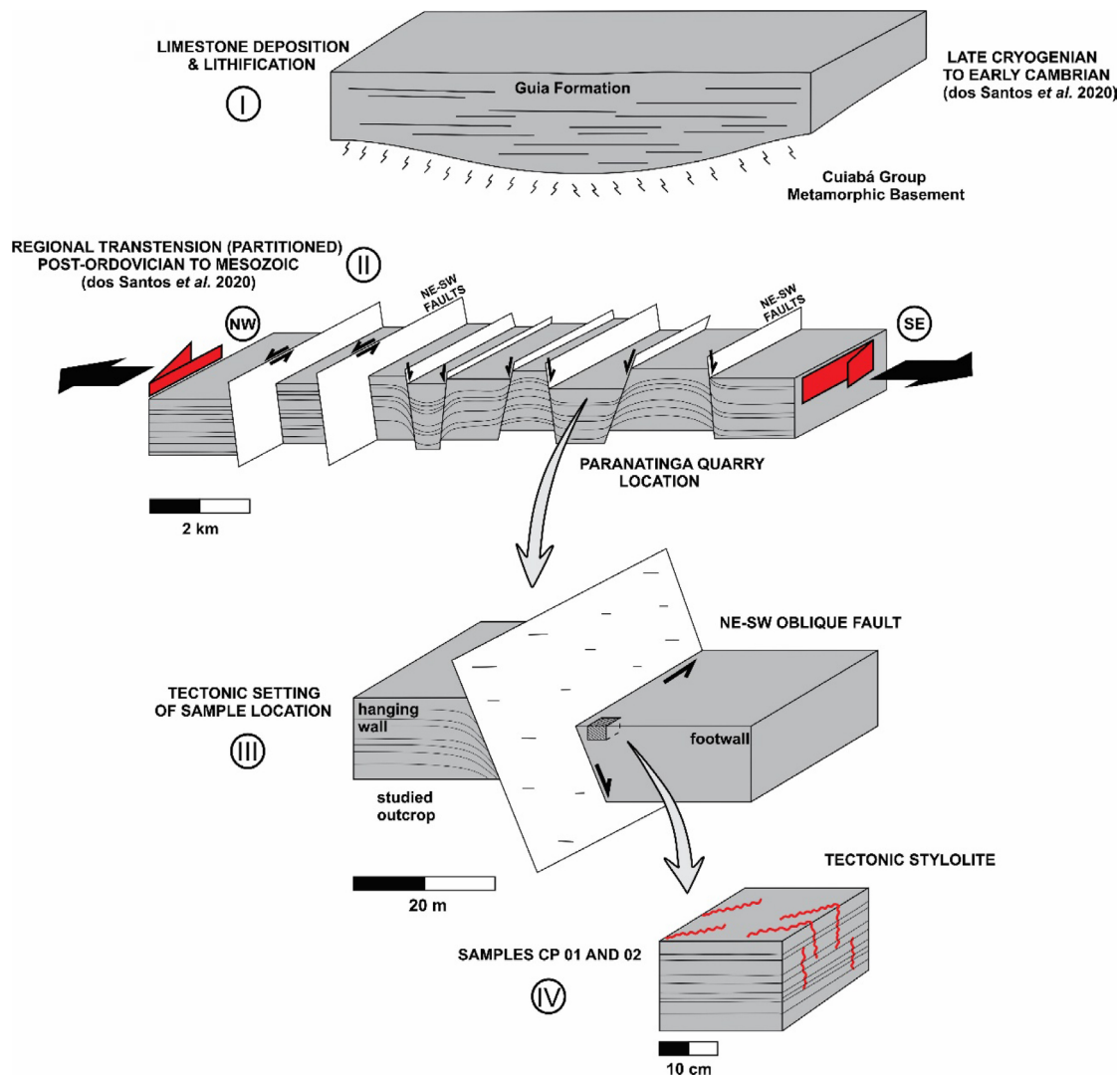


Figure 8. Schematic block diagram illustrating the regional transtension (partitioned). (I) We see the deposition and lithification of the Guia Formation limestones during the late Cryogenian to early Cambrian (Santos *et al.* 2020). (II) The regional transtension with oblique faults and the quarry location. (III) The outcrop-scale block shows the studied oblique faults that might have been triggered the stylolites formation. (IV) The sample-scale block displays the orthogonal relationship between the stylolites and the limestone bedding, which reinforces the perspective of tectonic stylolites.

perspective, the tectonic stylolites are interpreted as the result of the post-Ordovician transitional brittle deformation described by Santos *et al.* (2020) that affected the Araras Group (calcareous sequence) in the northern part of the Paraguay Belt. The late-Cryogenian to early-Cambrian carbonates were deformed during post-Ordovician transtension (Fig. 8), when NE-SW oblique normal and strike-slip faults were formed, according to Santos *et al.* (2020). These authors also described ENE-WSW normal faults of Ordovician-Silurian age in the Paraguay Belt, not observed in the studied rocks.

Quantitatively, the contractional strain value increases from the region with less to high stylolite concentration, from 3.29 to 16.9%. This suggests a correlation between the stylolite population density and the increasing value of total contractional strain (ϵ). The data agrees with the increasing values found by Benedicto and Schultz (2010), in mesostylolites.

Past decades of research defined stylolites as structures with a connectivity role either as a barrier or as a channel to fluid flux in reservoirs. According to Koehn *et al.* (2016), it will depend on the degree of stylolite roughness and the nature of the sealing material. In recent work, Bruna *et al.* (2019) suggest that the nature of the fluid circulating and the tectonic setting should also be taken into consideration. The studied stylolites probably play the role of channels for fluid flow according to the morphology described (e.g. high amplitude peak in the teeth).

As barriers, they could lead the fluids in a specific direction and thereby impose a meter-scale anisotropy to the reservoir. In general, the nature of this anisotropy would depend on stylolite orientation and the presence of one or several sets (e.g. a sedimentary and one or more tectonic sets).

A recommendation for future research is to better explore the nature of the filling material observed in stylolites, using more detailed and punctual chemical analysis. Furthermore, investigation on the stylolite-bearing limestone cementation may help to understand the evolution of a petroleum system (Ben-Itzhak *et al.* 2012, 2014). A better understanding of the total contractional strain (ϵ) in other areas of the Paraguay Belt regarding the Guia Formation might also prove to be an essential area for future work.

ACKNOWLEDGMENTS

This work was funded by Emal Mining Group and the first author is thankful to CAPES for the scholarship and was part of the project: “Tectônica e estratigrafia do sudeste da Faixa Paraguay (MT) e suas implicações com o Sistema Petrolífero Araras do Neoproterozoico”. We thank an anonymous reviewer for his thoughtful comments that improved an earlier version of the manuscript. H. Fossen is thanked for his thorough editorial handling of this manuscript.

ARTICLE INFORMATION

Manuscript ID: 20190136. Received on: 12/16/2019. Approved on: 12/01/2020.

K.S. wrote the first draft of the manuscript and prepared Figures 1, 3, 4, 5, 6, and 7; Tables 1, 2, and 3; F.B. provided advisorship regarding Paraguay Belt geology and tectonics, improved the manuscript through corrections and suggestions, plotted the data in stereograms, prepared Figures 2 and 8.

Competing interests: The authors declare no competing interests.

REFERENCES

- Almeida F.F.M. 1964. Geologia do Centro-Oeste Mato-Grossense. *Boletim da Divisão de Geologia e Mineralogia*, **53**.
- Almeida F.F.M. 1984. Província Tocantins, setor sudoeste. In: Almeida F.F.M., Hasui Y. (eds.). *O Pré-Cambriano do Brasil*. São Paulo: Blücher, p. 265-281.
- Alvarenga C.J.S. 1988. Turbiditos e a glaciação do final do Proterozoico Superior no cinturão dobrado Paraguay, Mato Grosso. *Revista Brasileira de Geociências*, **18**(3):323-327.
- Alvarenga C.J.S. 1990. *Phénomènes sédimentaires, structuraux et circulation de fluides développés à la transition chaîne-craton. Exemple de chaîne Paraguay d'âge protérozoïque supérieur, Mato Grosso, Brésil*. PhD Thesis, Université Aix-Marseille III, France, 177 p.
- Alvarenga C.J.S., Santos R.V., Dantas E.L. 2004. C-O-Sr isotopic stratigraphy of cap carbonates overlying Marinoan-age glacial diamictites in the Paraguay Belt, Brazil. *Precambrian Research*, **131**(1-2):1-21. <https://doi.org/10.1016/j.precamres.2003.12.006>
- Alvarenga C.J.S., Trompette R. 1993. Evolução tectônica brasileira da Faixa Paraguay: a estruturação da região de Cuiabá. *Revista Brasileira de Geociências*, **23**(1):18-30.
- Alvarenga C.J.S., Trompette R. 1994. A Faixa Paraguay e sua compartimentação estratigráfica e tectônica. In: Congresso Brasileiro de Geologia, 38, Camboriú. *Anais... SBG*, p. 239-240.
- André G.C., Hibsich S., Fourcade M., Cathelineau S., Buschaert S. 2010. Chronology of fracture sealing under a meteoric fluid environment: Microtectonic and isotopic evidence of major Cenozoic events in the eastern Paris Basin (France). *Tectonophysics*, **490**(3):214-28. <https://doi.org/10.1016/j.tecto.2010.05.016>
- Babinski M., McGee B., Tokashiki C.C., Tassinari C.C.G., Saes G.S., Pinho F.E.C. 2018. Comparing two arms of an orogenic belt during Gondwana amalgamation: Age and provenance of the Cuiabá Group, northern Paraguay Belt, Brazil. *Journal of South America Earth Science*, **85**:6-42. <https://doi.org/10.1016/j.jsames.2018.04.009>
- Beaudoin N., Koehn D., Lacombe O., Lecouty A., Billi A., Ahanarov E., Parlangeau C. 2016. Fingerprinting stress: stylolite and calcite twinning paleopiezometry revealing the complexity of progressive stress patterns during folding-the case of the Monte Nero anticline in the Apennines, Italy. *Tectonics*, **34**:1687-1712. <https://doi.org/10.1002/2016TC004128>
- Benedicto A., Schultz R.A. 2010. Stylolites in limestone: magnitude of contractional strain accommodated and scaling relationships. *Journal of Structural Geology*, **32**(9):1250-1256. <https://doi.org/10.1016/j.jsg.2009.04.020>
- Ben-Itzhak L.L., Ahanarov E., Karcz Z., Kaduri M., Toussaint R. 2014. Sedimentary stylolite networks and connectivity in limestone: Large-scale field observations and implications for structure evolution. *Journal of Structural Geology*, **63**:106-123. <https://doi.org/10.1016/j.jsg.2014.02.010>
- Ben-Itzhak L.L., Ahanarov E., Toussaint R., Sagy A. 2012. Upper bound on stylolite roughness as indicator for amount of dissolution. *Earth and Planetary Science Letters*, **337-338**:186-196. <https://doi.org/10.1016/j.epsl.2012.05.026>

- Brouste A., Renard F., Gratier J.P., Schmittbuhl J. 2007. Variety of stylolites' morphologies and statistical characterization of the amount of heterogeneities in the rock. *Journal of Structural Geology*, **29**(3):422-434. <https://doi.org/10.1016/j.jsg.2006.09.014>
- Bruna P.-O., Lavenu A.P.C., Matoni C., Bertotti G. 2019. Are stylolites fluid-flow efficient features? *Journal of Structural Geology*, **125**:270-277. <https://doi.org/10.1016/j.jsg.2018.05.018>
- Carozzi A.V., Vonbergen D. 1987. Stylolitic Porosity in Carbonates - a Critical Factor for Deep Hydrocarbon Production. *Journal of Petroleum Geology*, **10**(3):267-282. <https://doi.org/10.1111/j.1747-5457.1987.tb00946.x>
- Dawson W.C. 1988. Stylolite porosity in carbonate reservoirs. In: Annual Meeting of the American Association of Petroleum Geologists, 1988. *Proceedings...* 1988.
- Dunham R.J. 1962. Classification of carbonate Rocks according to depositional texture. In: Ham W.E. (ed.). *Classification of carbonate Rocks*. American Association of Petroleum Geologists Memoir, p. 108-121.
- Dunnington H.V. 1954. Stylolite development post-dates rock induration. *Journal of Sedimentary Petrology*, **24**(1):27-49. <https://doi.org/10.1306/D4269648-2B26-11D7-8648000102C1865D>
- Ebner M., Grasemann B. 2006. Divergent and convergent non-isochoric deformation. *Journal of Structural Geology*, **28**(10):1725-1733. <https://doi.org/10.1016/j.jsg.2006.07.008>
- Ebner M., Koehn D., Toussaint R., Renard F. 2009. The influence of rock heterogeneity on the scaling properties of simulated and natural stylolites. *Journal of Structural Geology*, **31**(1):72-82. <https://doi.org/10.1016/j.jsg.2008.10.004>
- Farr T.G., Rosen P.A., Caro E., Crippen R., Duren R., Hensley S., Kobrick M., Paller M., Rodriguez E., Roth L., Seal D., Shaffer S., Shimada J., Umland J., Werner M., Oskin M., Burbank D., Alsdorf D. 2007. The Shuttle Radar Topography Mission. *Review of Geophysics*, **45**:RG2004. <https://doi.org/10.1029/2005RG000183>
- Fossen H., Hesthammer J. 1997. Geometric analysis and scaling relations of deformation bands in porous sandstone. *Journal of Structural Geology*, **19**(12):1479-1493. [https://doi.org/10.1016/S0191-8141\(97\)00075-8](https://doi.org/10.1016/S0191-8141(97)00075-8)
- Gingras M.K., MacMillan B., Balcom B.J. 2002. Visualizing the internal physical characteristics of carbonate sediments with magnetic resonance imaging and petrography. *Bulletin of Canadian Petroleum Geology*, **50**(3):363-369. <https://doi.org/10.2113/50.3.363>
- Harris N.B. 2006. Low-Porosity Haloes at Stylolites in the Feldspathic Upper Jurassic Ula Sandstone, Norwegian North Sea: An Integrated Petrographic and Chemical Mass-Balance Approach. *Journal of Sedimentary Research*, **76**(3):444-459. <https://doi.org/10.2110/jsr.2006.040>
- Karcz Z., Scholz C.H. 2003. The fractal geometry of some stylolites from the Calcare Massiccio Formation, Italy. *Journal of Structural Geology*, **25**(8):1301-1316. [https://doi.org/10.1016/S0191-8141\(02\)00173-6](https://doi.org/10.1016/S0191-8141(02)00173-6)
- Katsman R., Aharonov E. 2006. A study of compaction bands originating from cracks, notches and compacted defects. *Journal of Structural Geology*, **28**(3):508-518. <https://doi.org/10.1016/j.jsg.2005.12.007>
- Klimczak C., Schultz R.A., Parashar R., Reeves D.M. 2010. Cubic law with aperture length correlation: implications for network scale fluid flow. *Hydrogeology Journal*, **18**:851-862. <https://doi.org/10.1007/s10040-009-0572-6>
- Klößen F. 1828. *Beitrag zur Mineral. U. Geol. Kenntnis: der Mark Brandenburg*. Bd.
- Koehn, D., Ebner, M., Renard, F., Toussaint, R., Passchier, C.W. 2012. Modelling of stylolite geometries and stress scaling. *Earth and Planetary Science Letters*, 104–113.
- Koehn D., Renard F., Toussaint R., Passchier C.W. 2007. Growth of stylolite teeth patterns depending on normal stress and finite compaction. *Earth and Planetary Science Letters*, **257**(3-4):582-595. <https://doi.org/10.1016/j.epsl.2007.03.015>
- Koehn D., Rood M.P., Beaudoin N., Chung P., Bons P.D., Gomez-Rivas E. 2016. A new stylolite classification scheme to estimate compaction and local permeability variations. *Sedimentary Geology*, **346**:60–71.
- Kostrov B. 1974. Seismic moment and energy of earthquakes, and seismic flow of rock. *Izvestiya Physics of the Solid Earth*, **13**:13-21.
- Lacerda Filho J.V., Souza J.O., Oliveira C.C., Ribeiro P.S.E., Boas P.F.V., Ibuquerque M.C., Frasca A.A.S., Borges F.R., Moreton L.C., Martins E.G., Camargo M.A., Valente C.R., Pimentel M.M., Botelho N.F. 2001. Geologia e Evolução Tectônica da Região Norte do Mato Grosso (Projeto Promin-Alta Floresta) In: Simpósio de Geologia da Amazônia, 7, 2001, Belém. *Anais...* SBG/Núcleo Norte.
- Molnar P. 1983. Average regional strain due to slip on numerous faults of different orientations. *Journal of Geophysical Research*, **88**:6430-6432.
- Nogueira A.C.R. 2003. *A plataforma carbonática Araras no sudeste do cráton amazônico, Mato Grosso: Estratigrafia, contexto paleoambiental e correlação com os eventos glaciais do Neoproterozóico*. PhD Thesis, Universidade de São Paulo, São Paulo, 173 p.
- Nogueira A.C.R., Riccomini C., Sial A.N., Moura C.A.V., Fairchild T.R. 2003. Soft-sediment deformation at the Neoproterozoic Puga cap carbonate (southwestern Amazon Craton, Brazil): confirmation of rapid icehouse to greenhouse transition in snowball Earth. *Geology*, **31**(7):613-616. [https://doi.org/10.1130/0091-7613\(2003\)031%3C0613:SDATBO%3E2.0.CO;2](https://doi.org/10.1130/0091-7613(2003)031%3C0613:SDATBO%3E2.0.CO;2)
- Olson J.E. 2003. Sublinear scaling of fracture aperture versus length: an exception or the rule? *Journal of Geophysical Research*, **108**(B9):2413. <https://doi.org/10.1029/2001JB000419>
- Park W.C., Schot E.H. 1968. Stylolites: their nature and origin. *Journal of Sedimentary Petrology*, **38**(1):175-191. <https://doi.org/10.1306/74D71910-2B21-11D7-8648000102C1865D>
- Passchier C.W., Trouw R.A.J. 2004. *Microtectonics*. New York: Springer, 306 p.
- Peacock D.C.P., Azzam I.N. 2006. Development and scaling relationships of a stylolite population. *Journal of Structural Geology*, **28**(10):1883-1889. <https://doi.org/10.1016/j.jsg.2006.04.008>
- Pimentel M.M., Fuck R.A., Jost H., Ferreira Filho C.F., Araújo S.M. 2000. The basement of the Brasília Fold Belt and Goiás Magmatic arc. In: Cordani U.G., Milani E.J., Thomaz Filho A., Campos D.A. (eds.). *Tectonic evolution of South America. 31st International Geological Congress*. Rio de Janeiro, p. 195-229.
- Railsback L.B. 1993. Lithologic controls on morphology of pressure-dissolution surfaces (Stylolites and dissolution seams) in Paleozoic carbonate rocks from the Midwestern United-States. *Journal of Sedimentary Petrology*, **63**(3):513-522.
- Raynaud S., Carrio-Schaffhauser E. 1992. Rock Matrix Structures in a Zone Influenced by a Stylolite. *Journal of Structural Geology*, **14**(8-9):973-980. [https://doi.org/10.1016/0191-8141\(92\)90028-U](https://doi.org/10.1016/0191-8141(92)90028-U)
- Renard F., Dysthe D. 2003. Pressure solution. In: Middleton G.V. (eds.). *Encyclopedia of Sediments and Sedimentary Rocks*. Dordrecht: Kluwer, p. 542-543.
- Renard F., Schmittbuhl J., Gratier J.P., Meakin P., Merino E. 2004. Three-dimensional roughness of stylolites in limestones. *Journal of Geophysical Research*, **109**(3):1-12. <https://doi.org/10.1029/2003JB002555>
- Ring U., Brandon M.T., Ramthun A. 2001. Solution-mass-transfer deformation adjacent to the Glarus Thrust, with implications for the tectonic evolution of the Alpine wedge in eastern Switzerland. *Journal of Structural Geology*, **23**(10):1491-1505. [https://doi.org/10.1016/S0191-8141\(01\)00015-3](https://doi.org/10.1016/S0191-8141(01)00015-3)
- Rolland A., Toussaint R., Baud P., Schmittbuhl J., Conil N., Koehn D., Renard F., Gratier J.P. 2012. Modeling the growth of stylolites in sedimentary rocks. *Journal of Geophysical Research, Solid Earth*, **117**(6):B06403. <https://doi.org/10.1029/2011JB009065>
- Rolland A., Toussaint R., Baud P., Conil N., Landrein P. 2014. Morphological analysis of stylolites for paleostress estimation in limestones. *International Journal of Rock Mechanics and Mining Science*, **67**:212-225. <https://doi.org/10.1016/j.ijrmms.2013.08.021>
- Santos I.M. dos, Pinheiro R.V.L., Holdsworth R.E., Nogueira A.C.R., Santos H.P., Domingos F.H.G. 2020. Basement-cover relationships and deformation in the Northern Paraguay Belt, central Brazil: implications for the Neoproterozoic-early Paleozoic history of western Gondwana. *Journal of the Geological Society*, **177**:475-491. <https://doi.org/10.1144/jgs2018-184>

- Scholz C.H. 1997. Earthquake and fault populations and the calculation of brittle strain. *Geowissenschaften*, **15**:124-130.
- Scholz C.H., Cowie P.A. 1990. Determination of total strain from faulting using slip measurements. *Nature*, **346**:837-839. <https://doi.org/10.1038/346837a0>
- Schultz R.A. 2003. Seismotectonics of the Amenthes Rupes thrust fault population, Mars. *Geophysical Research Letters*, **30**(6):1303. <https://doi.org/10.1029/2002GL016475>
- Schultz R.A. 2009. Scaling and paleodepth of compaction bands, Nevada and Utah. *Journal of Geophysical Research*, **114**:B03407. <https://doi.org/10.1029/2008JB005876>
- Schultz R.A., Klimczak C., Fossen H., Olson J.E., Exner U., Reeves D.M., Soliva R. 2013. Statistical tests of scaling relationships for geologic structures. *Journal of Structural Geology*, **48**:85-94. <https://doi.org/10.1016/j.jsg.2012.12.005>
- Schultz R.A., Soliva R., Fossen H., Okubo C.H., Reeves D.M. 2008. Dependence of displacement-length scaling relations for fractures and deformation bands on the volumetric changes across them. *Journal of Structural Geology*, **30**(11):1405-1411. <https://doi.org/10.1016/j.jsg.2008.08.001>
- Shaub B.M. 1939. The Origin of Stylolites. *Journal of Sedimentary Petrology*, **9**(2):47-61.
- Shaub B.M. 1949. Do stylolites develop before or after the hardening of the enclosing rocks. *Journal of Sedimentary Petrology*, **19**(1):26-36. <https://doi.org/10.1306/D426933C-2B26-11D7-8648000102C1865D>
- Silva Júnior J.B.C. 2011. *Sedimentação siliciclástica e proveniência do Grupo Alto Paraguay (Neoproterozóico-Cambriano), Borda sul do Cráton Amazônico e Faixa Paraguay Norte, Estado do Mato Grosso*. PhD Thesis, Universidade Federal do Pará, Belém, 126 p.
- Silva Júnior J.B.C., Nogueira A.C.R., Petri S., Riccomini C., Trindade R.I.F., Sial A.N., Hidalgo R.L. 2007. Depósitos litorâneos neoproterozóicos do Grupo Alto Paraguay no sudoeste do Cráton Amazônico região de Mirassol d'Oeste, Mato Grosso. *Revista Brasileira de Geociências*, **37**(3):595-606.
- Sternlof K.R., Rudnicki J.W., Pollard D.D. 2005. Anticrack inclusion model for compaction bands in sandstone. *Journal of Geophysical Research*, **110**:B11403. <https://doi.org/10.1029/2005JB003764>
- Stockdale P.B. 1922. Stylolites: their nature and origin. *Indiana University Studies*, **9**:1-97.
- Stockdale P.B. 1926. The stratigraphic significance of solution in rocks. *Journal of Geology*, **34**(5):399-414.
- Stockdale P.B. 1943. Stylolites: Primary or secondary? *Journal of Sedimentary Petrology*, **13**(1):3-12. <https://doi.org/10.1306/D4269175-2B26-11D7-8648000102C1865D>
- Sturm R. 2003. SHEARCALC a computer program for the calculation of volume change and mass transfer in a ductile shear zone. *Computers & Geosciences*, **29**(8):961-969. [https://doi.org/10.1016/S0098-3004\(03\)00093-1](https://doi.org/10.1016/S0098-3004(03)00093-1)
- Tapp B., Cook J. 1988. Pressure solution zone propagation in naturally deformed carbonate rocks. *Geology*, **16**(2):182-185. [https://doi.org/10.1130/0091-7613\(1988\)016%3C0182:PSZPIN%3E2.3.CO;2](https://doi.org/10.1130/0091-7613(1988)016%3C0182:PSZPIN%3E2.3.CO;2)
- Toussaint R., Aharanov E., Koehn D., Gratier P., Ebner M., Baud P., Rolland A., Renard F. 2018. Stylolites: a review. *Journal of Structural Geology*, **114**:163-195. <https://doi.org/10.1016/j.jsg.2018.05.003>
- Van Geet M., Swennen R., Wevers M. 2000. Quantitative analysis of reservoir rocks by microfocus X-ray computerized tomography. *Sedimentary Geology*, **132**(1-2):25-36. [https://doi.org/10.1016/S0037-0738\(99\)00127-X](https://doi.org/10.1016/S0037-0738(99)00127-X)
- Wright T.O., Platt L.B. 1982. Pressure dissolution and cleavage in Martinsburg shale. *American Journal Science*, **282**(2):122-135. <https://doi.org/10.2475/ajs.282.2.122>

Appendix I. Graphics.

